Research Article

Fabrication of pH-Responsive Chitosan/Polyvinylpyrrolidone Hydrogels for Controlled Release of Metronidazole and Antibacterial Properties

Zerihun Feyissa ⬤,[1] **Gemechu Deressa Edossa,**[1] **Tariku Bayisa Bedasa,**[1] **and Leta Guta Inki**[2]

[1]*Department of Applied Chemistry, School of Applied Natural Science, Adama Science and Technology University, P.O. Box 1888, Adama, Ethiopia*
[2]*Department of Applied Biology, School of Applied Natural Science, Adama Science and Technology University, P.O. Box 1888, Adama, Ethiopia*

Correspondence should be addressed to Zerihun Feyissa; zerefeyem@gmail.com

This research focused on preparing hydrogels with controlled drug release properties to control gastrointestinal tract bacterial infection. Chitosan (CS) and polyvinylpyrrolidone (PVP) were used as the base polymers, with the CS component crosslinked by glutaraldehyde for hydrogel preparation using the solution casting technique. The effect of varying glutaraldehyde content in the hydrogels was characterized by the extent of swelling in simulated physiological fluids of pH 1.2, 6.8, and 7.4; the development of porosity; and gel fraction. Functional groups and covalent and hydrogen bonds formed, thermal stability, phase structure, and morphology were characterized by Fourier-transform infrared spectroscopy, thermogravimetric analysis, X-ray diffraction, and scanning electron microscopy. The results show that the components in the hydrogels have good compatibility and formed honeycomb-like structures. In vitro studies confirmed that the hydrogels have good biodegradability at pH 7.4. Based on these properties, a CS/PVP hydrogel of the ratio of 60 : 40 crosslinked with 600 μL glutaraldehyde was selected for the in-situ loading of 200 mg of the drug metronidazole (MTZ). The hydrogel was characterized for cumulative drug release in the simulated physiological fluids and drug release kinetics using different models and for its antibacterial activity. The best-fit Korsmeyer–Peppas model suggests that MTZ release followed diffusion and swelling-controlled time-dependent non-Fickian transport related to hydrogel erosion. This hydrogel displays enhanced antimicrobial activity against *Staphylococcus aureus*, and *Escherichia coli* showed substantial inhibition zones indicating the produced CS/PVP hydrogels are promising candidates for controlled drug release applications.

1. Introduction

The leading cause of morbidity and mortality worldwide is associated with bacterial infections for which antibiotics are among the most frequently prescribed drugs [1, 2]. However, the conventional treatment methods of bacterial infections with antibiotics have certain inherent flaws in achieving optimal treatment. Repeated administrations of a particular drug, low quality drug formulations, and irrational use of drugs by patients, especially in developing countries, have been supposed to have led to increased risk of toxicity, overdose causing premature death, risk of hostile drug reactions, increase in health care costs, and development of antibiotic resistant bacteria [3].

Oral drug administrations based on controlled release systems using polymeric materials are a potential approach to deliver a specified dosage of the drug without any alternation in efficacy and to maintain the desired dosage in a sustained manner [4]. Hydrogels, which are three-dimensional crosslinked polymeric materials, achieved high attention in oral-controlled drug release applications. The properties of interest for hydrogels in such applications include the ability

to respond to external stimuli including the ability to display measurable volume change, pH, ionic strength, temperature, and electromagnetic field environment without dissolution [5, 6]. The ability of hydrogels to swell in physiological fluids enables the expansion of the polymer chains, allowing for the release of drugs and other bioactive agents entrapped in their structure. The presence of hydrophilic groups, such as –CONH, –OH, –CO, NH_2, –SO_3H, and –COOH, in the polymer network structure increases the affinity of hydrogels toward water [7, 8]. Hydrogels can contain more than 90% of their weight in the swollen state without dissolving based on the aqueous media and polymer compositions [9]. The synthesis likelihoods using different polymers and the manipulation of the resultant tri-dimensional chemically or physically crosslinked structures allow for the encapsulation or entrapment of drugs and their transport [10]. Such structures, with due manipulation of synthesis protocols, can be designed for high structural integrity and flexibility on swelling, and biodegradation can diminish the effect of hostile physiological environments on the drugs [11].

Hydrogels can be synthesized by crosslinking different natural or synthetic nontoxic and biocompatible polymer materials [12]. Some of the natural polymers that have been used to prepare hydrogels include chitosan (CS), alginate, pectin, guar gum, xanthan gum, and dextran [13, 14]. Synthetic polymers that can be used for the preparations of various hydrogels include polyacrylic acid (PAA), polymethacrylic acid (PMAA), polyvinyl alcohol (PVA), carboxymethyl cellulose (CMC), hydroxypropyl methylcellulose (HPMC), polyvinylpyrrolidone (PVP), and polyethylene glycol (PEG) [15, 16].

CS is composed of mainly β-$(1 \rightarrow 4)$ linked D-glucosamine and N-acetyl-D glucosamine units and extracted by alkaline deacetylation of chitin [17]. It is a natural linear polysaccharide that has been used in controlled drug delivery systems (CDDSs) owing to its biodegradability, nontoxicity, biocompatibility, and mucoadhesive nature [18, 19]. The primary amine (–NH_2) and hydroxyl (–OH) functional groups of CS allow the reactivity and easy modifications of its structure [20]. CS is soluble in an acidic environment through the protonation of its –NH_2 groups [21]. Irrespective of its benefits, CS exhibits poor mechanical strength [22]. The collapse of CS in an acidic environment and poor mechanical strength has led to the need for their modification by crosslinking with other biocompatible natural or synthetic polymers (e.g., PVP) to make stable networked essential material for use in CDDSs.

PVP produced by radical polymerization of N-vinylpyrrolidone monomer is a biocompatible, biodegradable, and water soluble synthetic polymer. It is a hydrophilic polymer widely used in biomedical applications for the production of microcapsules, tablets, and other medical devices [23]. However, PVP exhibits poor mechanical strength, hence, is subjected to rapid erosion, and has low stability in physiological conditions [24]. Consequently, burst and uncontrolled drug release take place, which further reduces the system efficiency as CDDSs [25]. It has tunable properties and can be crosslinked with natural polymers like CS, to develop a hydrogel system with improved properties for

use in DDSs [26]. When multiple component polymers (natural and/or synthetic) are crosslinked, the resulting polymeric networks show stable and synergistic properties (e.g., mechanical properties). Hybrid hydrogels are the subject of high interest to attain highly efficient performance, superior to their individual components in the CDDSs [27]. Crosslinked pH-responsive hydrogels have been utilized in the applications for the controlled release of various drugs. Yin et al. [28] prepared sodium alginate/CS nanocomposite for chondroitin sulfate release. Garakani et al. [29] fabricated CS/PVP hydrogel for controlled release of dexamethasone. Ata et al. [30] loaded cefixime to CS/PVP hydrogel for controlled release study. Vo et al. [22] prepared CS/poly (vinyl alcohol) for controlled release of amoxicillin.

Metronidazole (MTZ) is an effective antiprotozoal and antibiotic medicine, which is on the list of essential medicines worldwide [31]. It is used for the treatment of infections caused by anaerobic bacteria and various protozoan infections including giardiasis and trichomoniasis. It is available as immediate release in capsule and tablet forms, and no formulation for sustained and controlled release forms currently. The conventional oral administration of MTZ is associated with certain problems in delivering directly to the infectious site. The commonly reported side effects include anorexia, dizziness, nausea, transient neutropenia, peripheral neuropathy vomiting, and epigastric pain [32, 33]. Metallic taste and mouth dryness probably caused by the presence of high concentrations of the drug in the saliva and resistant bacteria strands development are reported [32, 34]. Therefore, developing controlled release MTZ delivery systems to decrease the dosing frequency and mitigate associated side effects by enhancing drug efficacy is needed.

This study reports the development of hydrogels using CS and PVP via the solution-casting process for the controlled release of MTZ using glutaraldehyde as a crosslinking agent. The polymer ratio (CS: PVP) and the crosslinker content were varied to formulate a hydrogel as a potent candidate for drug delivery applications. Fourier-transform infrared spectroscopy (FTIR), X-ray diffraction (XRD), field emission scanning electron microscopy (FESEM), and thermogravimetric analysis (TGA) characterized the hydrogels. Further, the hydrogels were analyzed for swelling behavior and biodegradation. The drug release profile and the release kinetics were established using a UV–visible spectrophotometer at 322 nm and different kinetic models. The qualitative antimicrobial activity was assessed for the MTZ-loaded hydrogel.

2. Experimental

2.1. Materials. CS ($\geq$75% deacetylated having bulk density of 0.15–0.3 g/cm^3 and viscosity >200 Cp) and PVP-30 (MW ~ 40,000 g/mol) were procured from Sisco Research Laboratory Pvt. Ltd (India). Glutaraldehyde solution (grade-II 25% in water), glacial acetic acid (99.75% trace metals basis), and ethanol were all purchased from Loba Chemie Pvt. Ltd (India). Pristine MTZ (β-lactam antibiotic) drug was provided by Ethiopian Pharmaceuticals Manufacturing Sh. Co. (EPHARM), Ethiopia. Sodium

hydroxide (NaOH), hydrochloric acid (HCl), sodium chloride (NaCl), potassium chloride (KCl), dibasic sodium phosphate (Na_2HPO_4), and potassium phosphate monobasic (KH_2PO_4) used for the preparation of the phosphate buffer solution (PBS), and Mueller–Hinton Agar (MHA; OXOID CM0337) were purchased from Sigma-Aldrich. Double distilled water (DDW) was used throughout this study.

2.2. Preparation of CS/PVP Hydrogels.

The CS/PVP hydrogels were prepared by the chemical crosslinking method [35]. According to the composition of the hydrogels (Table 1), CS was dissolved in 200 mL of 2% acetic acid aqueous solution at 50°C. PVP solutions were prepared separately by dissolving the requisite amounts in 200 mL of DDW. The two solutions were then mixed using an overhead stirrer at 500 rpm for 2 hours at 50°C. To the mixtures, 200 μL of 25% (v/v) glutaraldehyde was added under stirring at the same temperature until the formation of the gel. The reaction mass was then poured into glass Petri dishes and dried in a vertical double function thermostatic shaking incubator (LFZ-TSI series, China) at 40°C. The dried hydrogels were then stored in a desiccator to avoid moisture adsorption till required.

To evaluate the effect of crosslinker concentration, the hydrogel H2 (determined as optimal based on the swelling behavior in simulated physiological fluids) was also modified by varying the glutaraldehyde concentration (Table 2), employing the above procedure.

2.3. Preparation of MTZ-Loaded CS/PVP Hydrogel.

200 mg of MTZ was loaded into the hydrogel H2-G3 (determined as having the optimal swelling capacity in the simulated physiological fluids). CS (4.8 g) was dissolved in 200 mL of 2% (v/v) acetic acid aqueous solution at 50°C, and PVP (3.2 g) was dissolved separately in 200 mL of DDW. The two solutions were then mixed using an overhead stirrer at 500 rpm for 2 hours at 50°C. MTZ was dissolved in 100 mL of 0.1 M HCl solution and added slowly to the polymer mixture and stirred for 1 hour. Then, 600 μL of 25% (v/v) glutaraldehyde aqueous solution was added dropwise to the polymer-MTZ blend. The reaction mixture was stirred for a further 4 hours and then poured into a glass Petri dish followed by drying at 40°C in a vertical double function thermostatic shaking incubator (LFZ-TSI series, China). The dried drug-loaded hydrogel (MTZ-H2-G3) was stored in a desiccator to avoid moisture adsorption till required.

2.4. Preparation of Simulated Physiological Fluids.

Simulated physiological fluids including simulated gastric fluid (SGF), simulated intestinal fluid (SIF), and simulated colon fluid (SCF) were prepared using a previously reported procedure [36]. SGF was prepared by dissolving 2 g NaCl and 7 mL of 0.2 N HCl in DDW to a final volume of 1 L solution. The solution pH was then adjusted to 1.2 ± 0.1. SIF was prepared by dissolving 6.8 g of KH_2PO_4 and 0.94 g of NaOH in 1 L DDW, and the pH was adjusted to 6.8. SCF was prepared by dissolving 8 g NaCl, 0.2 g KCl, 1.15 g Na_2HPO_4, and

TABLE 1: Composition of CS/PVP hydrogels.

Hydrogel sample code	CS/PVP wt.% ratio (total polymer mass 8 g)		Glutaraldehyde volume (μL)
	CS	PVP	
H1	70	30	200
H2	60	40	200
H3	50	50	200
H4	40	60	200
H5	30	70	200

0.2 g KH_2PO_4 in DDW to a final volume of 1 L, and the pH was adjusted to 7.4 using 1 M HCl/1 M NaOH.

3. Characterization

3.1. Swelling Behavior.

To study the effect of CS : PVP ratio (Table 1) and crosslinker content (Table 2) on the pH-responsive nature of the prepared hydrogels, the swelling ratio was determined gravimetrically, in triplicate, by immersing a preweighed (W_i) 18 mm diameter hydrogel disc in each of the three simulated physiological fluids (SGF, SIF, and SCF) followed by incubation at 37°C while shaking at 100 rpm [30]. The hydrogel samples were removed from the simulated physiological fluids after time-defined intervals of up to 240 minutes, gently wiped between Whatman filter paper (grade 42), and weighed (W_t). This step was repeated until a constant mass of the hydrogel samples was obtained. The swelling ratio was calculated using equation (1):

$$\text{Swelling ratio (\%)} = (W_t - W_i)/W_i \times 100. \quad (1)$$

3.2. Porosity.

The ethanol solvent replacement method was used for the measurement of porosity [29]. The porosity of the hydrogels (Tables 1 and 2) was determined using a stoppered 25 mL beaker by taking the weight of the empty stoppered beakers as W_1. Pre-weighed hydrogel samples (W_h) were placed into the beakers, and 20 mL ethanol was added as an inert solvent to the beaker and weighted (W_2). After 24 hours, the hydrogel samples were removed, and the remaining components were weighed (W_3). The hydrogel pores full of ethanol were taken as the pore volume of the hydrogel samples. The porosity of the samples was calculated using equation (2), where ρ_e is the density of ethanol (g/cm^3):

$$\text{Porosity (\%)} = (W_2 - W_3 - W_h)/(W_1 - W_3 + 20\rho_e) \times 100. \quad (2)$$

3.3. Fourier-Transform Infrared Spectroscopy.

FTIR spectra of the pristine CS, PVP, MTZ, select hydrogels (H2-G2, H2-G3, and H2-G4), and the drug-loaded hydrogel (MTZ-H2-G3) were evaluated by an FTIR spectrometer (Alpha-T, Bruker, Germany). The samples were ground with KBr and compressed to prepare pellets. The analysis

TABLE 2: Hydrogel H2 modified by varying the concentration of glutaraldehyde.

Hydrogel sample code	CS/PVP wt.% ratio (total polymer mass 8 g)		Glutaraldehyde volume (μL)
	CS	PVP	
H2-G1	60	40	200
H2-G2	60	40	400
H2-G3	60	40	600
H2-G4	60	40	800
H2-G5	60	40	1000

was performed at a scanning rate of 120 scans/min in the wavelength range of 4000–400 cm^{-1} and resolution of 4 cm^{-1}.

3.4. X-Ray Diffraction. X-ray diffraction measurements of pristine CS, PVP, select hydrogels (H2-G2, H2-G3, and H2-G4), and the drug-loaded hydrogel (MTZ-H2-G3) were obtained by X-ray diffractometer (XRD-7000, SHIMADZU, Japan) with CuKα radiation source (1.5406 Å), steps at a scanning speed of 2θ 3°/min, an applied voltage of 40 kV, and current of 30 mA in the 2θ range 5–40° at room temperature.

3.5. Thermogravimetric Analysis. TGA of pristine CS, PVP, MTZ, and select hydrogels (H2-G2, H2-G3, and H2-G4), and hydrogel MTZ-H2-G3 was carried out using a DTA-TGA instrument (ATAT 2012, BJ HENVEN) at a heating rate of 15°C/min under nitrogen flow of 20 mL min^{-1} and within the temperature range of room temperature to 650°C.

3.6. Gel Fraction. The gel fraction of the prepared hydrogels (Tables 1 and 2), in triplicate, was determined as previously reported [37] with slight modification by immersing a known weight (W_0) of the samples in DDW for 48 hours at room temperature to leach out noncrosslinked polymer fractions. The extracted hydrogels were filtered, washed with a copious amount of DDW, and dried to constant weight (W_f) at 60°C. The gel fraction percentage was calculated using equation (3):

$$\text{Gel fraction (\%)} = W_f/W° \times 100. \tag{3}$$

3.7. In Vitro Biodegradation. The in vitro biodegradation of the hydrogels (Tables 2 and 3), the MTZ-loaded hydrogel, was evaluated gravimetrically by immersing pre-weighed (W_0) hydrogels in SCF (pH = 7.4) and incubated at 37.2°C while shaking at 80 rpm for 30 days [35]. After defined time intervals of 2–3 days, the hydrogels were removed from the SCF, properly wiped out using Whatman filter paper (grade 42) to remove the surface fluids, and weighed (W_f). The SCF was replaced with fresh solution after each measurement. The weight loss was calculated using equation (4):

$$\text{Weight loss (\%)} = (W_t - W°)/W° \times 100. \tag{4}$$

3.8. Field Emission Scanning Electron Microscopy. FESEM images were taken to examine the morphology of select hydrogels (H2-G2, H2-HG3, H2-G4, and H2-G5) and the drug-loaded hydrogel (MTZ-H2-G3) using an FESEM (ApreoS, Thermo Fisher Scientific, Singapore). Before imaging, the samples were coated with a thin film of gold.

3.9. In Vitro Drug Release Profile. The in vitro drug release profile of the hydrogel MTZ-H2-G3 was evaluated in triplicate by immersing the hydrogel in 50 mL of the simulated physiological fluids, SGF (pH 1.2), SIF (pH 6.8), and SCF (pH 7.4) and incubated at 37°C under constant shaking at 100 rpm [38]. The supernatant from each simulated physiological fluid was withdrawn at specified intervals and replaced with fresh simulated physiological fluids after each sample withdrawal. The absorbance was measured by a UV–visible spectrophotometer (Maalab Scientific Equipment Ltd., India) at 322 nm. The released drug concentration was determined against a calibration curve derived from standard solutions of MTZ (0.5–12 μg/mL) in 0.1 M HCl aqueous solution. The cumulative percentage concentration of drug release was determined using equation (5):

$$\text{Cumulative release (\%)} = C_t/C_1 \times 100, \tag{5}$$

where C_t is the amount of drug released at time t, and C_1 is the amount of MTZ loaded into the hydrogel.

3.10. Drug Release Kinetics. The kinetics and the mechanism of the in vitro MTZ release from the hydrogel (MTZ-H2-G3) were elucidated by fitting the release data into the zero-order model, first-order model, Higuchi model, and Korsmeyer–Peppas model.

3.11. Antibacterial Activity. The in vitro antibacterial activity of the hydrogel MTZ-H2-G3 was tested by an inhibition zone method using Staphylococcus aureus (ATCC25923) and Escherichia coli (ATCC25922). The test was carried out in MHA (OXOID CM0337) medium. The sterilized agar media were poured into Petri plates and allowed to solidify. On the surface of the media, fresh microorganism cultures (10^8 CFU/mL) were spread evenly. The hydrogel MTZ-H2-G3 was first sterilized using UV rays and then placed on nutrient agar in Petri dishes seeded with 20 μL of bacterial cell suspensions. The Petri dishes were examined for the zone of inhibition after 24 hours incubation at 37°C. The presence of a clear zone that formed around the sample on the plate medium was taken as an indication of inhibition against the bacterial species. The zone was measured using a ruler and reported as the zone of inhibition. The hydrogel H2-G3 was used as the negative control and the pristine MTZ as the positive control.

3.12. Statistical Analysis. All data are expressed as the mean ± standard derivation (SD). The data fitting and figures were made on OriginPro-2021 software.

4. Results and Discussion

The CS/PVP hydrogels were successfully synthesized by using glutaraldehyde as the crosslinking agent. The possible polymer–polymer and polymer–drug interaction mechanisms

TABLE 3: Drug release kinetics for MTZ from hydrogel MTZ-H2-G3.

pH	Zero-order model		First-order model		Higuchi model		Korsmeyer–Peppas	
	K	R^2	K	R^2	K	R^2	n	R^2
1.2	0.0232	0.8443	0.0716233	0.6652	0.1452	0.9604	0.5848	0.9814
6.8	0.0225	0.8772	0.0801444	0.7111	0.1382	0.9608	0.6347	0.9826
7.4	0.0217	0.8779	0.09212	0.7096	0.1327	0.9568	0.7264	0.9753

are shown in Schemes 1(a) and 1(b). In the hydrogel networks, glutaraldehyde crosslinks the amino ($-NH_2$) and hydroxyl ($-OH$) groups of the CS through hydrogen bonding, and PVP, which is a hydrophilic polymer, is interlaced to the hydrogel network through hydrogen bonding and physical interactions. The crosslinking between the CS chains and also due to the physical entanglement of PVP within the crosslinked CS chains forming dense semi-interpenetrating polymer networks (semi-IPNs) [39]. During the interactions, the ring structure of PVP can form empty spaces within the hydrogel film because of the random arrangement of the crosslinked hydrogel network. Similarly, MTZ, which is also a hydrophilic drug, is incorporated into the semi-IPN hydrogel system through different physical interactions, such as electrostatic and hydrogen bonding between polar groups of the drug and the polymer chains. The possible interaction mechanisms between CS and PVP have been reported in the literature [29, 40]. In the current study, the proposed chemical and physical interactions between the polymer components and the drug are further confirmed by FTIR analysis.

4.1. Swelling Behavior. The swelling behavior is helpful to understand the drug delivery mechanism, since a higher release is due to the greater extent of physiological fluids uptake, resulting in increased wetting and penetration into the hydrogel matrices and, in turn, increasing the diffusion of drugs. The swelling ratio (%) of the hydrogels H1 to H5 in SGF, SIF, and SCF is shown in Figures 1(a), 1(b), and 1(c). It is observed that the swelling ratio of the hydrogels follows a similar trend irrespective of the physiological fluid employed, however, with a different extent of absorption.

The swelling ratios were the highest in the acidic condition of SGF (pH 1.2), followed by the slightly acidic condition of SIF (pH 6.8), and the lowest in a slightly basic condition of SCF (pH 7.4). Hydrogel H5 with CS/PVP wt.% ratio of 30/70 shows the highest swelling ratios of ca. 535%, 520%, and 490% in SGF, SIF, and SCF, respectively, after 240 minutes. In contrast, the lowest values of ca. 475%, 450%, and 370% are for the hydrogel H1 with CS/ PVP wt.% of 70/30, respectively, in comparison. In acidic conditions, the behavior is due to the ionization and protonation balance of the tertiary $-NH2$ group in the hydrogels because of the charge repulsion [41] and the nitrogen of PVP, which leads to chain relaxation, faster hydrogen-bond dissociation, and, thus, higher SGF diffusion. The lower swelling in the mildly acidic conditions of SIF tends to be due to a lower level of chain relaxation and slower hydrogen-bond dissociation. In the slightly alkaline condition of SCF, the still lower swelling is mainly driven by diffusion,

but with the absence of the chain relaxation effect due to protonation of the amino groups as a quaternary ammonium salt with positive charges. This implies that as the pH increases (above pH 6), the amino groups become deprotonated, and repulsions in the polymer chains are reduced due to loss charge. Also, the reduced swelling is attributed to the increased hydrophobicity of the hydrogels with CS content at a higher pH value [42].

The higher swelling ratios of the hydrogels with increasing PVP content are associated with the more hydrophilic nature of PVP than CS [43]. Also, the pyrene ring in PVP is expected to create void volumes within the hydrogel structures, due to the irregular arrangement of the polymer chains in the matrices. As a result of the hydrogen bonding and electrostatic interactions between PVP and CS, there is a decrease in the number of hydrophilic functional groups, and on increasing the CS content, there is an increase in the availability of CS hydrophilic sites. During swelling, the simulated physiological fluids can easily diffuse into the hydrogel matrices and fill up the void volumes without the formation of hydrogen bonds.

In the initial stages of immersion of the hydrogels in the three physiological biological fluids, the observed swelling is due to water molecules of the fluids forming hydrogen bonds with the hydrophilic groups present in the polymer chains. More water then tends to surround this bound water to form clusters and finally, any excess water present enters freely into the gel network resulting in more swelling [24]. The amine and hydroxyl groups present on the CS backbone render the polymer unstable in wet environments as they are sites for a high affinity for water [44].

From the FTIR results (Figure 4.6) and other literature [45], it is evidenced that glutaraldehyde only enters into crosslinking reactions with the amino groups of the CS chains, and the PVP chains are physically entangled within the CS network through electrostatic interactions. On blending CS with PVP, the amine and hydroxyl groups of the CS interact with the carbonyl groups of PVP, leading to the formation of a tri-dimensional (3D) network in the matrices and a reduced affinity of CS for water [44].

The optimized hydrogel H2 with a typical composition of CS and PVP (ratio 60:40) was further evaluated for effect on swelling by increasing the crosslinking agent glutaraldehyde content (Table 2) 200 μL to 600 μL (hydrogels H2-G1, H2-G2, and H2-G3) results in a similar monotonic pH-dependent swelling behavior as for the hydrogels H1 to H5 except for the different extents of absorption which is seen to decrease [Figures 2(a), 2(b), and 2(c)]. A further increase in the glutaraldehyde content to 800 μL and 1000 μL results in a dramatic decrease in swelling even though the response to pH is similar. This observation is explained by porosity,
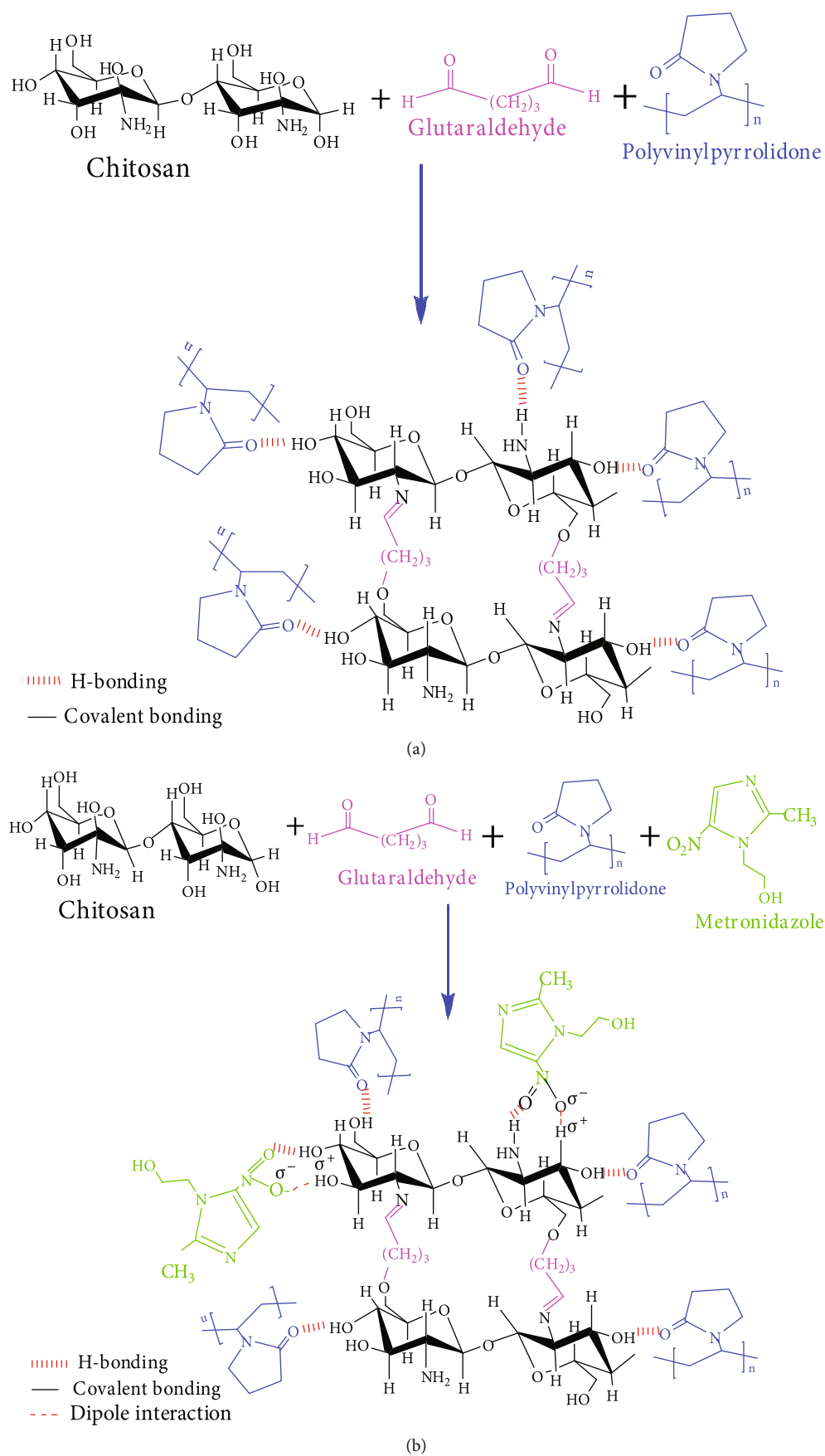
SCHEME 1: Schematic diagram indicating interactions of (a) CS and PVP polymers and (b) CS, PVP, and MTZ via glutaraldehyde crosslinker.
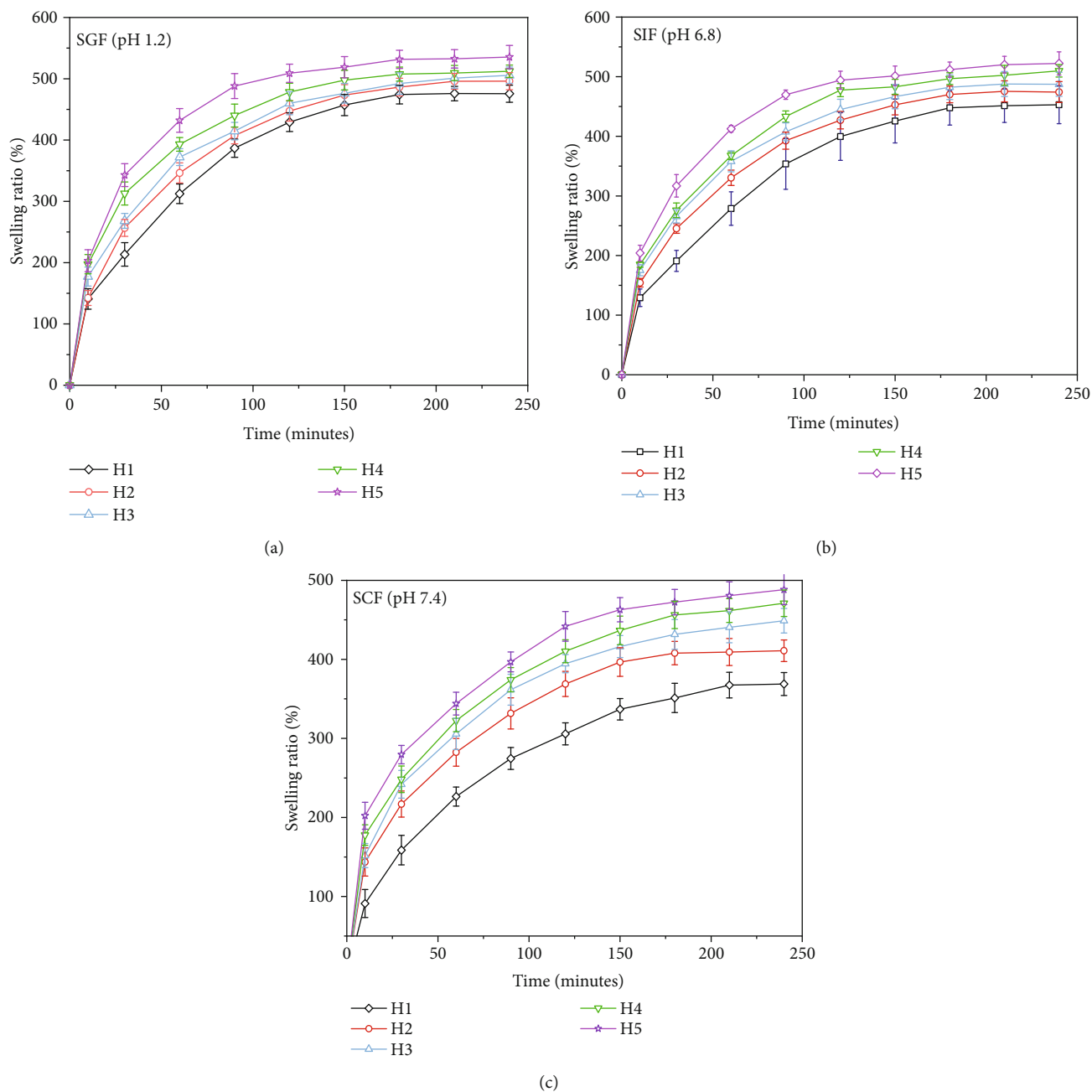
Figure 1: Swelling ratio of hydrogels H-1 to H-5 in (a) SGF, (b) SIF, and (c) SCF.

i.e., pore volume formation and its effects discussed in the next section.

4.2. Porosity. Porosity is an integral property of hydrogels intended for drug release applications because it affects the absorption capacity, affecting the drug's diffusion. It depends on the number of pores present in the network structure and, consequently, on the crosslinking density of the hydrogels. Figure 3(a) shows the porosity of the hydrogels H1 to H5, wherein a monotonic increase from ca. 61% to ca. 83% is obtained with increasing PVP content, respectively. This increase in porosity is attributed to the rise in the viscosity of the hydrogel solutions during preparation. As the viscosity

of the hydrogels increases with PVP content, the removal of bubbles from the matrices decreases to a certain extent. The bubbles prevented from escaping from the solutions result in the formation of interconnected channels, due to which porosity is increased. In the case of the hydrogels H1 to H5, the effect of crosslinking of CS with 150 μL glutaraldehyde does not supersede the viscosity effect, i.e., CS is partially crosslinked. The exact phenomenon is observed for the hydrogels H2-G1 to H2-G3 (Figure 3(b)), wherein the porosity increases in a monotonic manner from ca. 77% to ca. 95%, respectively.

However, as the content of glutaraldehyde increases to 800 μL and 1000 μL (hydrogels H2-G4 and H2-G5), the
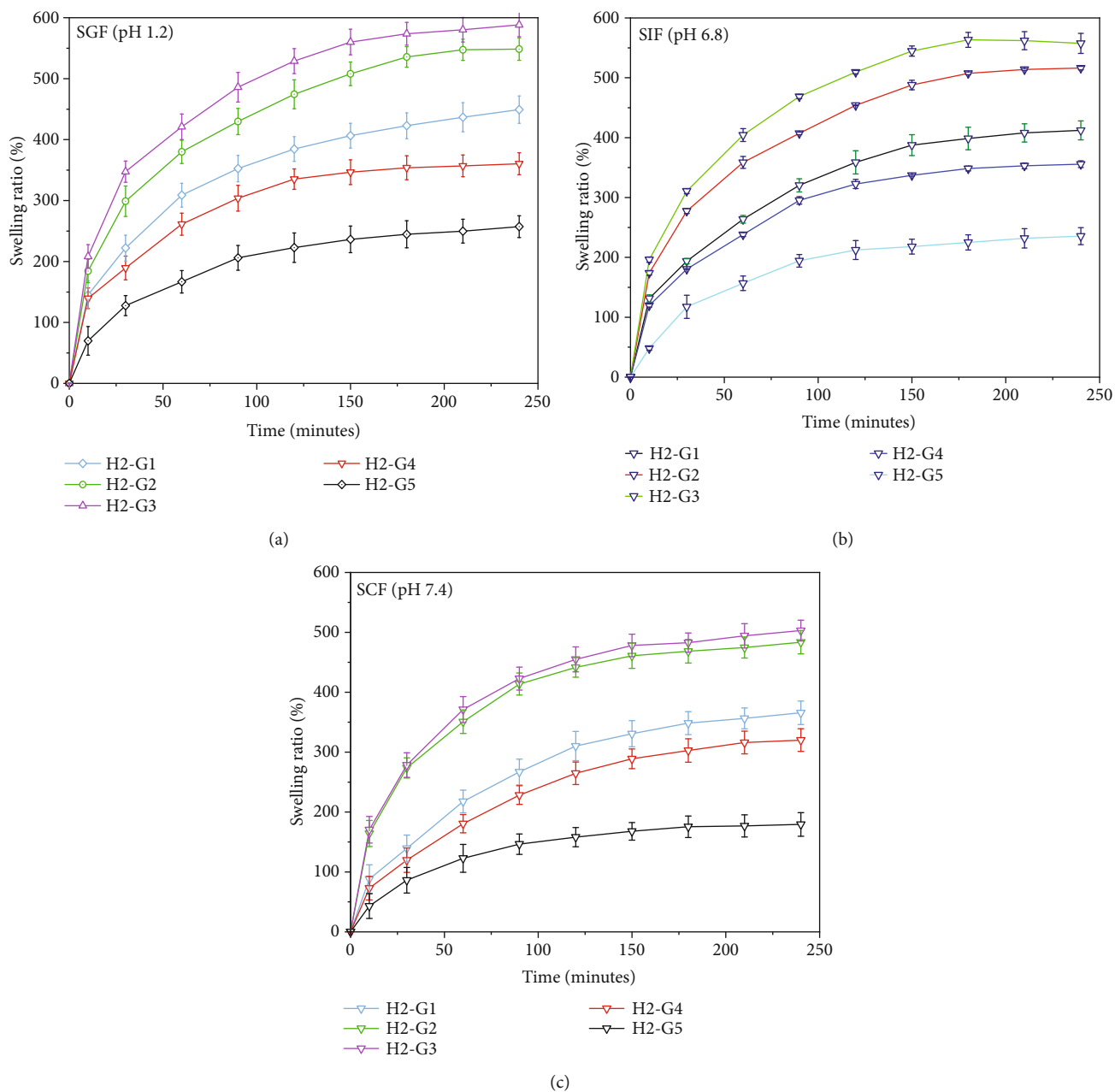
(a)

(b)

(c)

Figure 2: Swelling ratio of hydrogel H2 with increasing glutaraldehyde content in (a) SGF, (b) SIF, and (c) SCF.

porosity dramatically decreases to ca. 73% and ca. 64%, respectively, because of the increasing entanglement between CS and PVP due to the increasing crosslink density because of which the matrices of the hydrogels H2-G4 and H2-G5 form highly compact structures. The latter results also clearly indicate that crosslinking of CS with a glutaraldehyde content above 600 μL supersedes the viscosity effect leading to highly compact matrices. Based on the above observations, hydrogel H2-G3 was selected for the loading of MTZ.

4.3. FTIR Analysis. Figures 4(a) shows the FTIR spectra of pristine CS, PVP, and hydrogels H2-G1 to H2-G5. From Figure 4(a), it is observed that the spectrum of CS shows

a broad band of strong intensity between 3000 and 3600 cm^{-1}, attributed to overlapping stretching vibrations of the O–H groups and the N–H bonds of the primary amine groups of stretching vibrations. The peaks at 2920 and 2853 cm^{-1} are attributed to the C–H of the methyl (–CH3) groups and alkyl (–CH2–) chains [46]. Because of the incomplete degree of deacetylation of CS, the presence of chitin is observed by the amide carbonyl peak at 1600–1800 cm^{-1}.

The peaks at approximately 1637, 1554, 1315, and 605 cm^{-1} are assigned to amides I, II, and III, and N–H out-of-plane vibration, respectively [47]. The peaks at 1418 and 1381 cm^{-1} are assigned to the CH3 symmetrical deformation mode. Peaks corresponding to the saccharide structure of CS
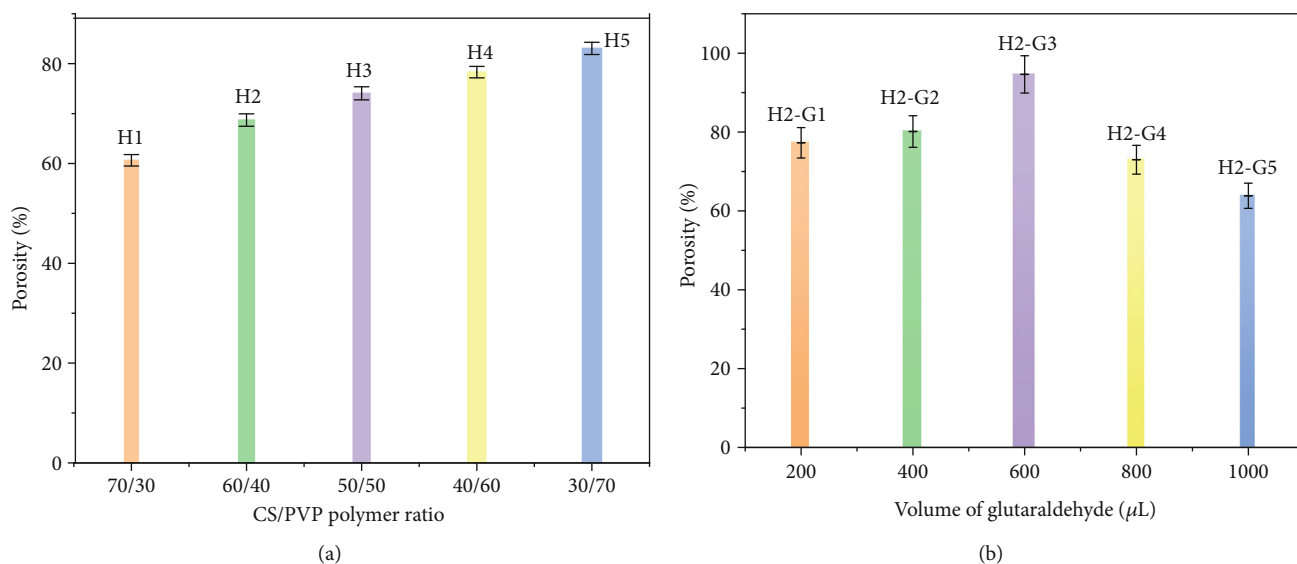
(a)

(b)

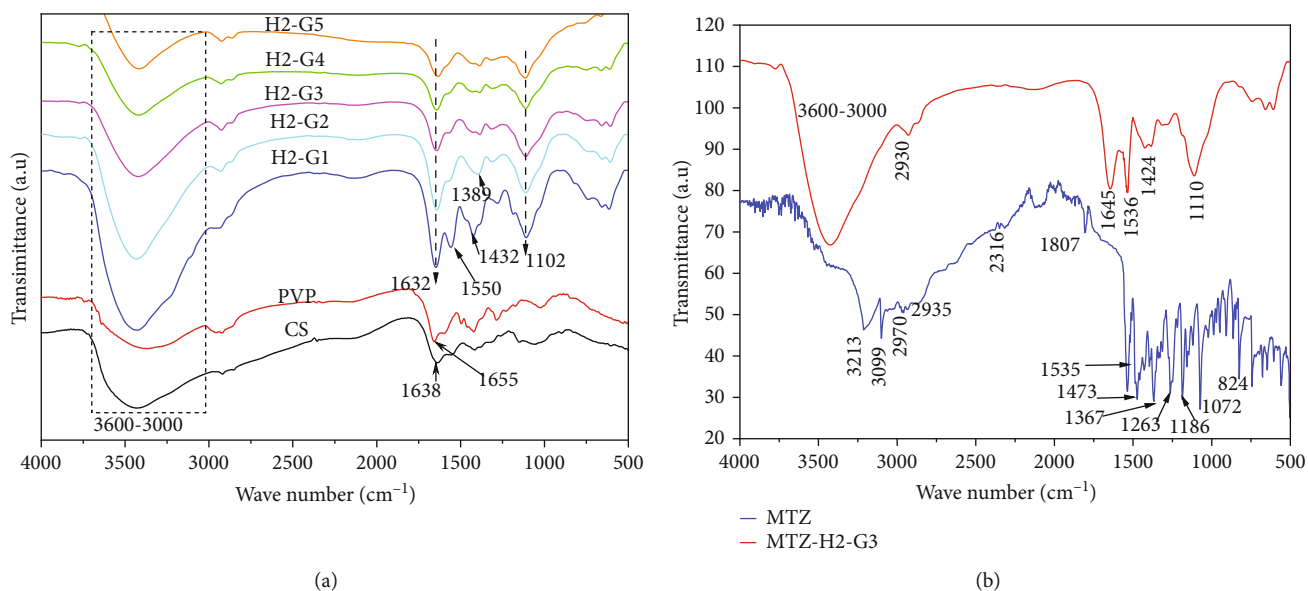FIGURE 3: Porosity of hydrogel (a) H1 to H5 and (b) H2-G1 to H2-G5.

(a)

(b)

FIGURE 4: FTIR spectra of (a) pristine CS, PVP, and hydrogels H1-G1 to H2-G5 (b) pristine MTZ and hydrogel MTZ-H2-G3.

are at 1150 and 897 cm^{-1} [48]. The FTIR spectrum of pristine PVP shows a broad band between 3600 and 3000, corresponding to the O–H stretching vibration of moisture due to the polymer's inherent hygroscopic nature [49]. Peaks at 2923, 1655, 1495, 1423, 1285, and 1024 cm^{-1} are assigned to CH2 symmetric stretching, –C=O (confirm it) stretching vibrations, C–H bending, CH2 wagging, frequency of C–N, and out-of-plane rings of CH_2 bending (rocking), respectively [49, 50]. The peak at 1655 cm^{-1} also shows the hygroscopic nature of the polymer. The spectra of the crosslinked hydrogels H2-G2, H3-G3, and H3-G4 show that upon crosslinking of CS with increasing glutaraldehyde amount, the band sharpens between 3000 and 3600 cm^{-1} and is attributed to the use of acetic acid as a solvent, protonating the NH_2 group, which reduces the CS–aldehyde crosslinking (Scheme 1(a)) [51].

Figure 4(b) shows the FTIR spectra of pristine MTZ and MTZ-H2-G3 hydrogel. From Figure 4(b), it is observed that the spectrum of pristine MTZ shows an absorption band between 3221 attributed to stretching vibrations of the O–H groups, peak at 3099 cm^{-1} is due to the stretching vibration of imidazole (C=C–H) [52, 53], the peaks at 2937 and 2853 cm^{-1} are attributed to the stretching of the C–H of the methyl (–CH3) and alkyl (–CH2–) groups [54]. The peaks at 1807 cm^{-1} and 1473 cm^{-1} are due to asymmetric N–O stretching and symmetric stretching of NO_2 bonds. The peaks at 1535 and 1367 cm^{-1} (nitroso N–O stretching), 1263 cm^{-1} (–C=C–), 1186 cm^{-1} (–C=N stretching), 1072 cm^{-1} (C–O stretching), 824 cm^{-1} (C–H stretching) [15, 52].

The FTIR spectra are observed in the MTZ-H2-G3 at 1645 cm^{-1} (C=O stretching), 1110 cm^{-1} (benzene ring C–H
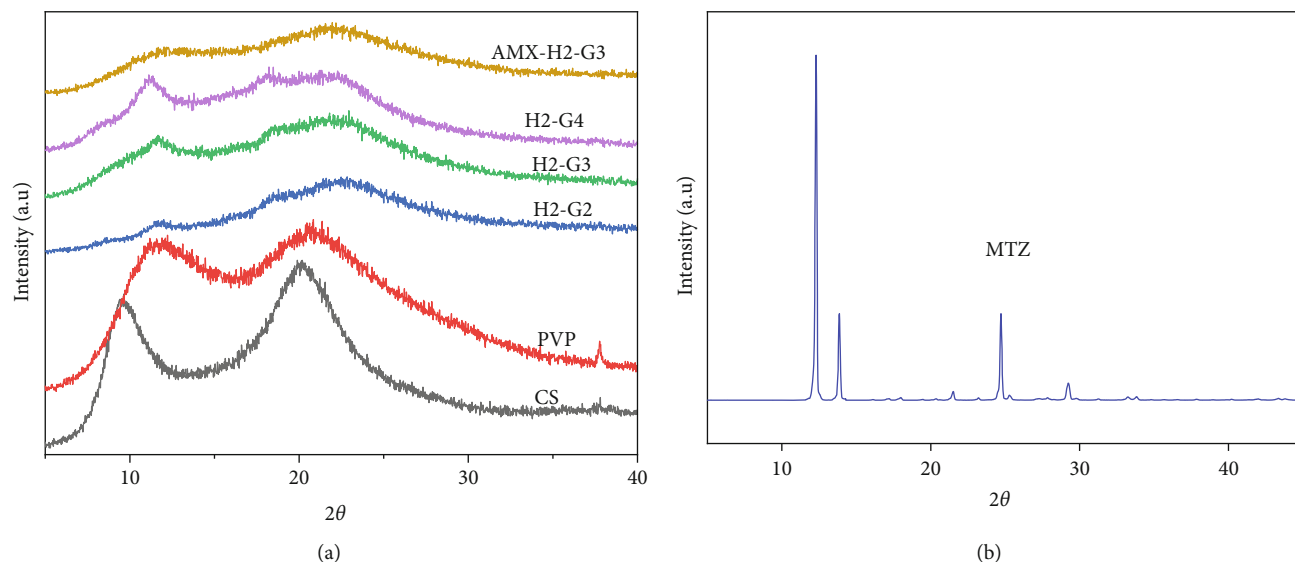
(a)

(b)

FIGURE 5: XRD diffractograms of (a) pristine CS, PVP, and hydrogels H2-G2 to H2-G4 and MTZ-H2-G3 (b) pristine MTZ.
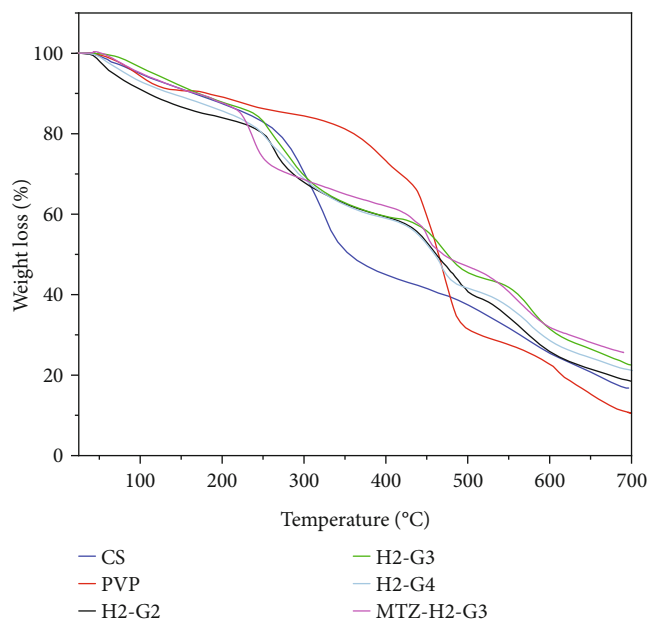

FIGURE 6: TGA thermograms of pristine CS and PVP, hydrogels H2-G2 to H2-G4 and MTZ-H2-G3.

deformation vibration), and $1424\,cm^{-1}$ (C–H bond bending vibrations). The newly appeared peak at $1536\,cm^{-1}$ is due to the N–O bond stretching of MTZ, confirming the presence of MTZ in the hydrogel, and the absence of other peaks of MTZ in the hydrogel shows the presence of interactions between the polymers and the drug (Scheme 1(b)) [54]. The result indicates the stability of MTZ in the hydrogel. The interaction of MTZ with the hydrogel matrix occurs via this end, which reveals MTZ is successfully incorporated into the hydrogel through different physical interactions such as hydrogen bonding.

4.4. X-Ray Diffraction. Figure 5(a) shows the XRD patterns of the pristine CS, pristine PVP, hydrogel H2-G3, and

MTZ-H2-G3. The diffraction pattern of pristine CS shows the typical crystalline peaks of the polymer with four peaks at 2θ values of 9.6°, 20.2°, 21.3°, and 38.7° corresponding to (020), (200), (201), and (143) diffraction planes, respectively [55]. The first two peaks at 2θ values of 9.6° and 20.2° are slightly lower than the α and β crystal forms of CS implying that they are the hydrated form of CS [56], and the pattern is in good agreement with JCPDS 39-1894. For pristine PVP, two peaks at 2θ values of 11.6° and 20.6° are observed. The first peak is due to scattering produced by the presence of short-range order in the amorphous regions, whereas the second is due to a pseudocrystalline phase [57]. The diffraction pattern of the hydrogel H2-G3 is very much different, in that, the first peak of CS, which depends on the water quantity (020), is reduced due to the crosslinking of the polymer with glutaraldehyde. This indicates that the dialdehyde is altering the species responsible for water bonding [58]. The crystalline region of CS having almost disappeared with the appearance of broad bands, indicating the amorphous morphology of the hydrogels due to strong interactions between CS and PVP [59].

Figure 5(b) shows diffraction pattern of pristine MTZ with peaks at 2θ values of 12.3°, 13.8°, 24.7°, and 29.3°. The pattern is similar to those reported in the literature for the drug [60, 61]. The drug loading caused to decrease in the crystallinity of the hydrogel system. The appearance of a broader peak confirms the amorphous structure of the drug-loaded hydrogel systems, which shows the molecular miscibility and interaction between the drug and the components.

4.5. Thermogravimetric Analysis. The primary thermograms of pristine CS, PVP, and select hydrogels H2-G2 to H2-G4 and MTZ-H2-G3 are shown in Figure 6. CS shows three distinct degradation steps. The first mass loss step of ca. 7% up to 105°C is due to the loss of easily removed free water, which does not interact via secondary interactions. A gradual slope follows this till 214°C with a further mass loss of
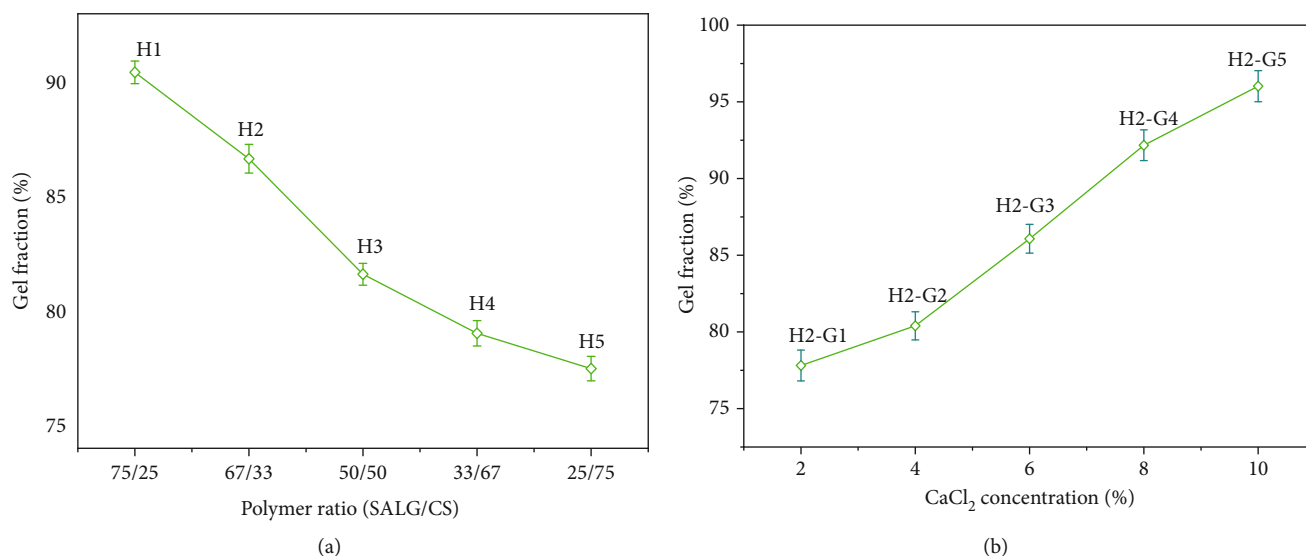
(a)

(b)

Figure 7: Gel fraction of (a) hydrogels H1 to H5 as a function of CS/PVP ratio and (b) hydrogels H2-G1 to H2-G5 as a function of glutaraldehyde content.
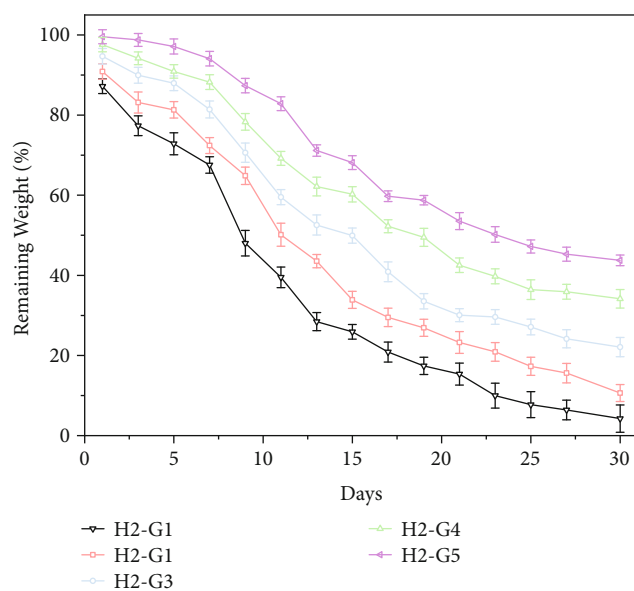

Figure 8: In vitro degradation of hydrogels H2-G1 to H2-G5 in SCF (pH 7.4) at 37°C for 30 days.

ca. 8% due to loss of bound water. The second mass loss step of ca. 32% in the range of 214–367°C is because of the partial degradation of the polymer, and the third step to 700°C is due to complete degradation with a final remaining mass of ca. 17%.

PVP also shows three degradation steps. The first mass loss step of 9% between 45°C and 135°C is due to the loss of adsorbed water followed by a slope between 135°C and 238°C with a mass loss of ca. 5% due to evaporation of bound water. The second mass loss step of ca. 56% between 238°C and 508°C is due to the partial degradation of the polymer, and the third step to 700°C is due to total degradation with a final remaining mass of 10%. Thermograms of the hydrogels H2-G32, H2-G3, and H2-G4 show that mass

loss occurs in four steps. The first and second step mass loss is due to the loss of the free water, which is easily removed as it is noninteracting up to 110°C, above which the removal of freezing water forms weak forces with both CS and PVP, and bound water entering into hydrogen bonding with the polymer chains occurs [17, 62, 63]. The thermogram of MTZ-H2-G3 shows four degradation steps. The first mass loss occurred between 33°C and 175°C, which attributed to the loss of free water with weight loss of about ca. 10%. The second step weight loss was observed between 175°C and 238°C with weight loss of ca. 16% corresponding to the decomposition of the polymers. The third and last thermal degradation steps appeared between 533°C and 700°C with a final weight residue of 26% attributed to the total degradation of the polymers [60].

The observed thermal stability of these events is also related to the covalent bonds formed between CS and glutaraldehyde and the hydrogen bonding interactions with PVP [59]. The third mass loss step is due to the disruption of the secondary forces between the polymer chains of CS and PVP, and also with glutaraldehyde along with partial degradation of the polymers, whereas the fourth mass loss step is due to the total degradation of the hydrogels.

4.6. Gel Fraction. The covalent crosslinking of polymer chains represented by the gel fraction is inversely associated with the toughness of a polymeric network [64, 65]. CS matrices, in pure form, are fragile and exhibit uncontrollable porosity and rapid dissolution in the stomach's acidic environment. It restricts their use for drug delivery by the oral route because of the limited capacity for controlling drug release [42]. Similarly, hydrogels of PVP alone display poor mechanical properties and swelling behaviors. Blending PVP with CS enables the preparation of hydrogels that exhibit properties, such as the control of the porous nature, that are prerequisites for drug release applications. Also, the extent of crosslinking of CS in such blends influences
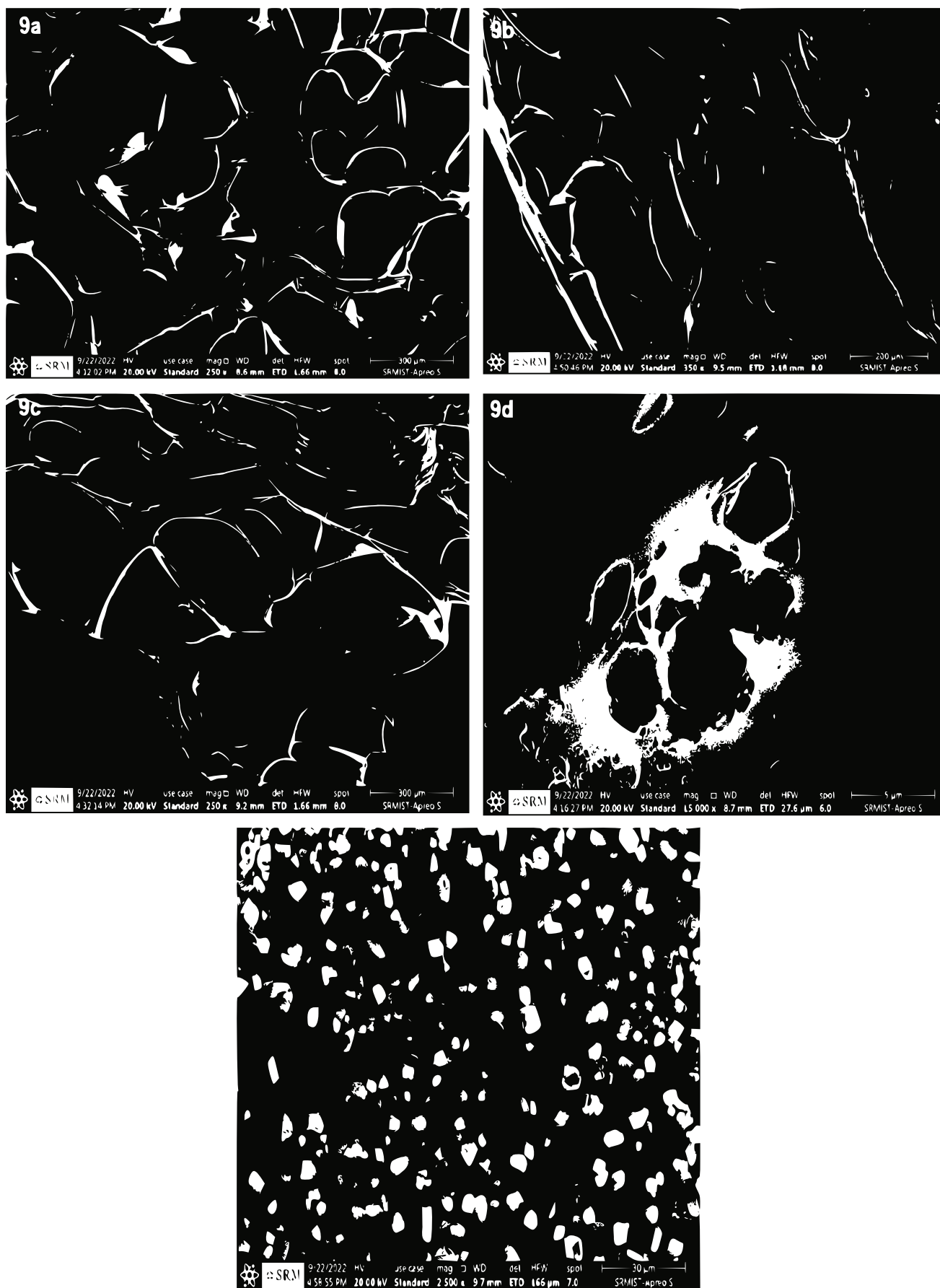
FIGURE 9: FESEM micrographs of (a, b, c, and d) hydrogels H2-G3 to H2-H5 and (e) hydrogel MTZ-H2-H3.
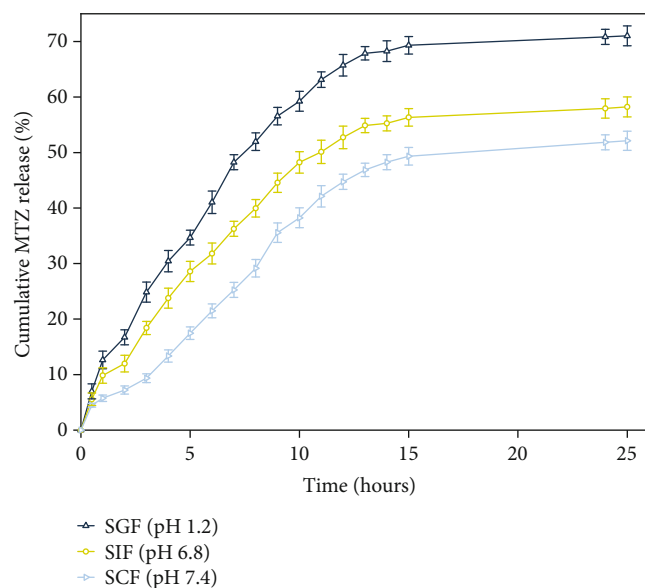
Figure 10: Cumulative MTZ release from the hydrogel MTZ-H2-G3 in SGF, SIF, and SGF at 37°C.

the integrity of the hydrogel structure and, in turn, affects the mechanical and swelling properties.

Figures 7(a) and 7(b) show the gel fraction of the hydrogels H1 to H5 and H2-G1 to H2-G5, respectively. From Figures 7(a) and 7(b), monotonic decrease in gel fraction from ca. 82% for the hydrogel H1 to ca. 71% for the hydrogel H5 is seen.

The values of the gel fraction of the hydrogels show that crosslinking CS with glutaraldehyde occurs during hydrogel synthesis; it decreases due to the increasing PVP content, which is highly soluble in water. Moreover, the decrease is not significant within a range of ca. 11%, implying that at a constant glutaraldehyde content of 150 μL and as the CS content decreases, enhanced crosslinking of the CS phase may be expected, which does not supersede the viscosity effect. Figure 7(b) shows that as the glutaraldehyde content in hydrogel H2 (CS/PVP ratio 60:40) is increased from 200 μL (H2-G1) to 1000 μL(H2-G3), there is an increase in gel fraction within a range of ca. 17% from ca. 79% (H2-G1) to ca. 96% (H2-G5). The obtained values indicate that CS is partially crosslinked, even though with a high gel fraction of ca. 86%, at a glutaraldehyde content of 600 μL (H2-G3) and almost completely crosslinked at a glutaraldehyde content of 1000 μL. The high rigidity of hydrogels H2-G4 and H2-G5 due to their high gel fractions is reflected by the dramatic decrease in their swelling ratio and porosity due to the restricted movement of polymer chains [66].

4.7. In Vitro Biodegradation.

Figure 8 shows the in vitro degradation of the hydrogels H2-G1 to H2-G5 immersed in SCF (pH 7.4) at 37°C for 30 days as a function of increasing glutaraldehyde content. It is observed that the hydrogels show similar degradation behavior, the only difference being a reduction in weight loss with increasing glutaraldehyde content. The weight loss behavior also indicates that irrespective of the glutaraldehyde content, the rate of degradation

between day 1 and day 7 is relatively slower, followed by a maximum rate between day 7 and day 17. Between days 17 and 30, the degradation rate begins to taper. CS alone in wet environments is unstable due to the presence of amine and hydroxyl groups in its structure, which have a high affinity for water leading to hydrolytic degradation of the polymer [44].

PVP is soluble in water, but when blended with CS, the –NH2 and –OH groups of CS interact with the –C=O groups of PVP to form a compact three-dimensional network in the blend leading to a reduced affinity for water. It has also been shown that CS and PVP can form a helical conformation in solution rendering them a slight hydrophobic property because of the CH groups and their stereoregularity [29].

The reduced affinity for water is further enhanced by crosslinking of CS in the CS–PVP hydrogels, which in the present results increases with glutaraldehyde content. This implies that there will still be some noninteracting –NH2 groups in CS despite forming increasingly compact structures on crosslinking. The remaining noninteracting –NH2, –OH, and –C=O groups are responsible for the hydrolytic degradation of the hydrogels [44, 67], and the degradation occurs through the scission of interchain linkages of CS, PVP, and glutaraldehyde (amine bonds of CS covalently linked glutaraldehyde) and dissociation of secondary interactions.

4.8. Morphology.

FESEM micrographs of the surface of the hydrogels H2-G2 to H2-G5 and MTZH2-G3 are shown in Figures 9(a), 9(b), 9(c), 9(d), and 9(e). The surface morphology of the hydrogels H2-G2 to H2-G5 (Figures 9(a), 9(b), 9(c), and 9(d)) shows that as the glutaraldehyde content increases from 400 to 600 μL (H2-G4), the size of the open channel-like porous structures increases. Further increasing the content of glutaraldehyde from 800 μL (H2-G4) to 1000 μL (H2-G5) decreases the pore size. The hydrogels H2-G2, H2-G3, H2-G4, and H2-G5 show a pore diameter size distribution of ca. $81 \pm 20 \mu$m, $132 \pm 42 \mu$m, $44 \pm 21 \mu$m, and $32 \pm 17 \mu$m, respectively.

FESEM micrographs of the surface of the hydrogels MTZ-H2-G3 [Figure 9(e)] appear to be compact due to their filling with drug particles. The surface structure of the hydrogel MTZ-H2-G3 confirms the interactions between the hydrogel and MTZ. The pores in the structural areas of the hydrogels are regions through which water permeates and serves as sites for interaction with external stimuli and the loaded drug in the hydrogels. The micrograph of MTZ-H2-G3 shows that MTZ particles are present in the pores and on the surface of the hydrogel. The systems appear to be compact due to their filling with drug particles. The drug particles within the pores do not appear agglomerated but if any it is very low.

4.9. In Vitro Drug Release.

Figure 10 shows the cumulative release profiles of the drug MTZ from MTZ-H2-G3 in SGF, SIF, and SCF at 37°C as a function of time for 25 hours. The drug release in the first 1 hour is ca. 12.6%, 9.8%, and 6% in SGF, SIF, and SCF, respectively. After that, the release gradually follows a monotonic pattern with

TABLE 4: Antibacterial activity of hydrogel MTZ-H2-G3.

| No | Bacterial strain | Zone inhibition diameter of test samples (mm) ± SD | | |
		Hydrogel H2-G3 (negative control)	MTZ (positive control)	Drug-loaded hydrogel MTZ-H2-G3
1	*Staphylococcus aureus* (ATCC25923)	10.21 ± 0.897	13.72 ± 1.26	20.82 ± 1.12
2	*Escherichia coli* (ATCC25922)	9.73 ± 0.786	11.63 ± 0.654	23.46 ± 1.31

time, irrespective of the simulated physiological fluid pH. At 25 hours, the cumulative drug release is ca. 71%, 58%, and 52% in SGF, SIF, and SCF, respectively, showing the expected influence of the medium pH since CS is a pH-sensitive polysaccharide based on its swelling properties. In MTZ-H2-G3, the porosity is related to its structure's diffusion coefficient since the size dimensions of the drug MTZ particles are dispersed on the surface and pores of the hydrogel observed from the FESEM micrograph (Figure 9(e)). Furthermore, the release pattern will also depend on the extent of the solubility of the drug in the different simulated physiological fluids.

The residual groups of crosslinked CS in SGF [pH below its pK_a (ca. 6.4)] get protonated and form hydrogen bonds with water molecules. An increase follows in the electrostatic repulsion between the protonated –NH2 groups of the CS network and an expansion of the vacant space between the chains. This expansion leads to the swelling of the polymer and increases the MTZ release in SGF (pH 1.2) [40]. The pyrrolidine rings of PVP in the hydrogel provide free volumes in the structure of the hydrogel, allowing more space for water molecules [29]. In comparison, in SIF and SCF (pH 6.8 and 7.4), the polymer chains deprotonate and condense; thus, the drug release is slower. Furthermore, delayed MTZ release from the hydrogel is due to interactions of –C=O groups in the PVP structure with the –NH2 and –OH groups of CS structures and –OH and NO_2 of MTZ. Only when there is an optimal ratio between the content of CS and PVP do both polymers contribute to the prolonged release of MTZ.

4.10. Drug Release Kinetics. To evaluate the release mechanism of MTZ from MTZ-H2-G3, the cumulative percent release data were fitted into different release kinetic models such as the zero-order, first-order, Higuchi, and Korsmeyer–Peppas models. Table 3 shows the corresponding result of each linear fitted model of the release rate of MTZ in SGF, SIF, and SCF as a function of time. The highest coefficient of correlation (R^2) was used to select the model that best fits the drug's release pattern. The release kinetics of MTZ in SGF shows that the R^2 value of the Korsmeyer–Peppas (0.9814) is greater than the Higuchi model (0. 9604), zero-order model (0.8443), and first-order model (0.6652). These results show that the Korsmeyer–Peppas model is the best suited for the release of MTZ. Similarly, in SIF and SCF, the Korsmeyer–Peppas model shows the highest R^2 value of 0.9826 and 0.9753, respectively, and is again the best-fit kinetic model for the release of MTZ.

Furthermore, the calculated diffusional exponent "n" for the release of MTZ in SGF, SIF, and SCF by the Korsmeyer–Peppas

model is 0.5848, 0.6347, and 0.7268, respectively. Since the exponent $n > 0.45$, the diffusion and relaxation rates are similar. The model suggests that the drug release follows the physical phenomenon of diffusion and swelling-controlled time-dependent non-Fickian transport ($0.45 < n < 0.85$) related to erosion of the hydrogel [68].

4.11. Antibacterial Activity. The antibacterial activity of the hydrogel MTZ-H2-G3 against *S. aureus* (ATCC25923) and *E. coli* (ATCC25922) is shown in Table 4.

Figures 11(a) and 11(b) show the photographs of the inhibition zones of the pristine MTZ (positive control), H2-G3 (negative control), and MTZ-H2-G3 with significant inhibitory growth against the bacteria species. The drug loaded hydrogel (MTZ-H2-G3) inhibited the *S. aureus* and *E. coli* bacteria with zones of inhibition ranging between 20.82 ± 1.12 and 23.46 ± 1.31 mm, respectively (Table 4). This shows that the drug-loaded hydrogel system is successful in inhibiting the growth of these bacteria species. The observed inhibition zone of the unloaded hydrogel is due to the antibacterial nature of CS. CS binds to the bacterial DNA via its cationic amine groups inhibiting protein and mRNA synthesis of the bacterial species [69]. Its antibacterial activity is directly proportional to its degree of deacetylation (in this study, CS is ≥75% deacetylated), which in turn is related to the number of the protonated amine groups. MTZ is a class of nitroimidazole drug that interacts with the DNA of bacteria forming nitroso radicals and hydroxyl amine derivatives leading to the loss of helical structure of DNA and hence causes cell death of the susceptible organisms [70]. The higher inhibition zone of the drug-loaded hydrogel (MTZ-H2-G3) than the pristine drug (PC) against both *S. aureus* and *E. coli* shows the synergistic effects between MTZ and the hydrogel MTZ-H2-G3 in addition to the antibacterial nature of CS [71]. From these results, the MTZ-loaded CS/PVP hydrogel had promising potential for use in CDDSs.

5. Conclusion

Crosslinked CS/PVP pH-sensitive hydrogels with different ratios of the polymers and glutaraldehyde concentrations were prepared, and a composition was applied for the controlled MTZ release. FTIR clarified all the functional groups of CS and PVP in the hydrogels, and well-defined crosslinking and hydrogen bonding was observed. The swelling behavior of the hydrogels in the simulated physiological solutions of different pH values showed that they were both CS/PVP ratio and glutaraldehyde concentration-dependent and pH-sensitive. These parameters also influenced the porosity and gel content, as seen by microscopy and extraction

(a)
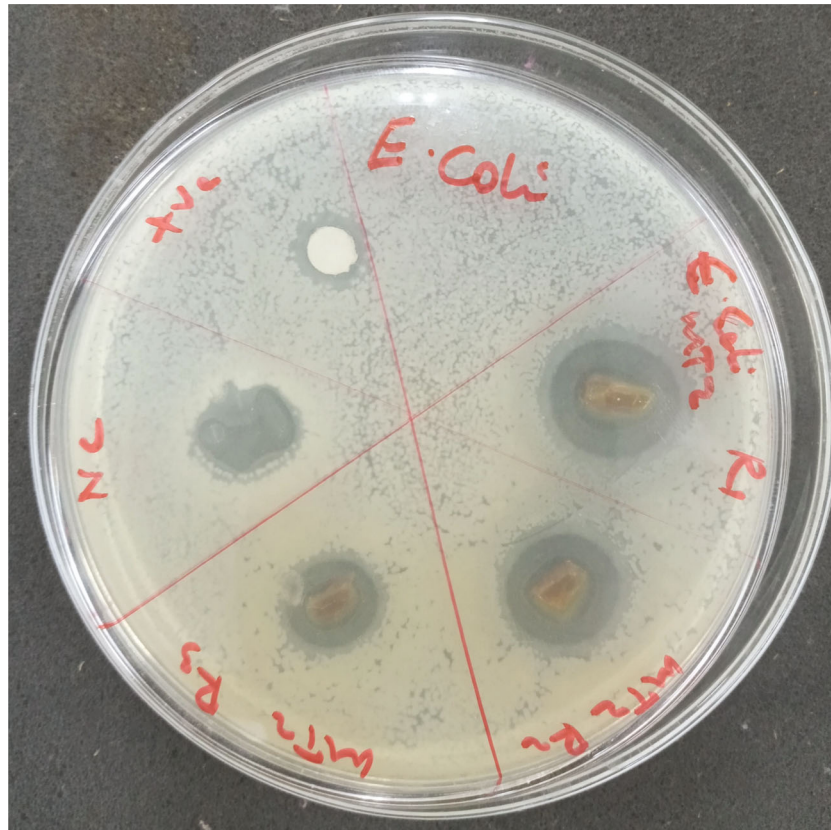
(b)

FIGURE 11: Disc diffusion assays showing zone of inhibition exhibited by unloaded H2-G3 (NC), MTZ-H2-G3, and pure metronidazole (pc) against (a) *Staphylococcus aureus* and (b) *Escherichia coli*.

results. The transformation of the phases to the amorphous nature of the hydrogels with increasing glutaraldehyde concentration is seen by XRD. The thermal stability of the hydrogels is better than CS alone. The hydrogel composition for MTZ loading was chosen based on its swelling behaviors, biodegradability, and glutaraldehyde concentration, showing good drug release characteristics in basic conditions and enhanced antibacterial activity. It is envisaged that this developed composition and further study can provide an efficient CDDS.

Data Availability

The data that support the findings of this study are available from the corresponding author, Zerihun Feyissa, upon request.

Conflicts of Interest

The authors declare that they have no conflicts of interest.

Acknowledgments

References

[1] B. C. Mindt and A. DiGiandomenico, "Microbiome modulation as a novel strategy to treat and prevent respiratory infections," *Antibiotics*, vol. 11, no. 4, p. 474, 2022.

[2] C. Dolecek, S. Shakoor, B. Basnyat, T. Okwor, and B. Sartorius, "Drug-resistant bacterial infections: we need urgent action and investment that focus on the weakest link," *PLoS Biology*, vol. 20, no. 11, article e3001903, 2022.

[3] D. Mamo and B. K. Alemu, "Rational drug-use evaluation based on World Health Organization Core drug-use indicators in a tertiary referral hospital, Northeast Ethiopia: a cross-sectional study," *Drug, Healthcare and Patient Safety*, vol. 12, pp. 15–21, 2020.

[4] T. Rajesh, "Controlled release drug formulation in pharmaceuticals: a study on their application and properties," *World Journal of Pharmaceutical Research.*, vol. 5, no. 2, pp. 1704–1720, 2016.

[5] M. Tian, J. Zhou, X.-J. Qi, and R. Shen, "Thermo-sensitive hydrogel and their biomedical applications," *IOP Conference Series*, vol. 714, no. 3, p. 032062, 2021.

[6] L. Osorno, A. N. Brandley, D. T. Maldonado, A. Yiantsos, R. J. Mosley, and M. E. Byrne, "Review of contemporary self-assembled systems for the controlled delivery of therapeutics in medicine," *Nanomaterials*, vol. 11, no. 2, p. 278, 2021.

[7] A. Majeed, F. Pervaiz, H. Shoukat, K. Shabbir, S. Noreen, and M. Anwar, "Fabrication and evaluation of pH sensitive chemically cross-linked interpenetrating network [gelatin/polyvinylpyrrolidone-co-poly(acrylic acid)] for targeted release of 5-fluorouracil," *Polymer Bulletin*, vol. 79, no. 1, pp. 1–20, 2020.

[8] S. H. Zainal, N. H. Mohd, N. Suhaili, F. H. Anuar, A. M. Lazim, and R. Othaman, "Preparation of cellulose-based hydrogel: a review," *Journal of Materials Research and Technology*, vol. 10, pp. 935–952, 2021.

[9] T. L. Rapp and C. A. DeForest, "Targeting drug delivery with light: a highly focused approach," *Advanced Drug Delivery Reviews*, vol. 171, pp. 94–107, 2021.

[10] A. Onaciu, R. Munteanu, A. Moldovan, C. Moldovan, and I. Berindan-Neagoe, "Hydrogels based drug delivery synthesis, characterization and administration," *Pharmaceutics*, vol. 11, no. 9, p. 432, 2019.

[11] M. Bustamante-Torres, D. Romero-Fierro, B. Arcentales-Vera, K. Palomino, H. Magaña, and E. Bucio, "Hydrogels classification according to the physical or chemical interactions and as stimuli-sensitive materials," *Gels*, vol. 7, no. 4, p. 182, 2021.

[12] Y. Hu, "A double-layer hydrogel based on alginate-carboxymethyl cellulose and synthetic polymer as sustained drug delivery system," *Scientific Reports*, vol. 11, no. 1, 2021.

[13] R. Cazorla-Luna, A. Martín-Illana, F. Notario-Pérez, R. Ruiz-Caro, and M.-D. Veiga, "Naturally occurring polyelectrolytes and their use for the development of complex-based mucoadhesive drug delivery systems: an overview," *Polymers*, vol. 13, no. 14, p. 2241, 2021.

[14] K. Ghosal and S. D. Ray, "Alginate/hydrophobic HPMC (60M) particulate systems: new matrix for site-specific and controlled drug delivery," *Brazilian Journal of Pharmaceutical Sciences*, vol. 47, no. 4, pp. 833–844, 2011.

[15] A. K. Nayak and M. S. Hasnain, *Advanced Biopolymeric Systems for Drug Delivery*, pp. 373–384, Springer, Cham, Switzerland, 2020.

[16] P. Bhatt, S. Trehan, N. N. Inamdar, V. K. Mourya, and A. Misra, *Polymers in drug delivery: an update*, pp. 1–42, Elsevier, Netherlands, 2021.

[17] N. Gull, S. M. Khan, O. M. Butt et al., "Inflammation targeted chitosan-based hydrogel for controlled release of diclofenac sodium," *International Journal of Biological Macromolecules*, vol. 162, pp. 175–187, 2020.

[18] R. H. Sizilio, "Chitosan/PVP-based mucoadhesive membranes as a promising delivery system of betamethasone-17-valerate for aphthous stomatitis," *Carbohydrate Polymers*, vol. 190, pp. 339–345, 2018.

[19] F. Tentor, G. Siccardi, P. Sacco, D. Demarchi, and E. Marsich, "Long lasting mucoadhesive membrane based on alginate and chitosan for intravaginal drug delivery," *Journal of Materials Science: Materials in Medicine*, vol. 31, no. 3, pp. 1–12, 2020.

[20] S. E. Gerami, M. Pourmadadi, H. Fatoorehchi, F. Yazdian, H. Rashedi, and M. N. Nigjeh, "Preparation of pH-sensitive chitosan/polyvinylpyrrolidone/α-Fe2O3 nanocomposite for drug delivery application: emphasis on ameliorating restrictions," *International Journal of Biological Macromolecules*, vol. 173, pp. 409–420, 2021.

[21] M. C. G. Pellá, M. K. Lima-Tenório, E. T. Tenório-Neto, M. R. Guilherme, E. C. Muniz, and A. F. Rubira, "Chitosan-based hydrogels: from preparation to biomedical applications," *Carbohydrate Polymers*, vol. 196, pp. 233–245, 2018.

[22] T. M. T. Vo, T. Piroonpan, C. Preuksarattanawut, T. Kobayashi, and P. Potiyaraj, "Characterization of pH-responsive high molecular-weight chitosan/poly(vinyl alcohol) hydrogel prepared by gamma irradiation for localizing drug release," *Bioresources and Bioprocessing*, vol. 9, no. 1, pp. 1–15, 2022.

[23] A. Rasool, S. Ata, and A. Islam, "Stimuli responsive biopolymer (chitosan) based blend hydrogels for wound healing application," *Carbohydrate Polymers*, vol. 203, pp. 423–429, 2019.

[24] S. Jana and S. Jana, *Interpenetrating Polymer Network*, pp. 1–20, Springer Pte. Limited, Singapore, 2020.

[25] Z. Zou, B. Zhang, X. Nie et al., "A sodium alginate-based sustained-release IPN hydrogel and its applications," *RSC Advances*, vol. 10, no. 65, pp. 39722–39730, 2020.

[26] M. Kurakula and G. K. Rao, "Pharmaceutical assessment of polyvinylpyrrolidone (PVP): as excipient from conventional to controlled delivery systems with a spotlight on COVID-19 inhibition," *Journal of Drug Delivery Science and Technology*, vol. 60, p. 102046, 2020.

[27] K. Wang, Y. Hao, Y. Wang, and J. Chen, "Functional hydrogels and their application in drug delivery, biosensors, and tissue engineering," *International Journal of Polymer Science*, vol. 2019, 14 pages, 2019.

[28] X. B. Yin, Q. Yu, B. Li, and C. D. Zhang, "Preparation and characterization of sodium alginate/chitosan composite nanoparticles loaded with chondroitin sulfate," *Advances in Materials Science and Engineering*, vol. 2021, 9 pages, 2021.

[29] S. S. Garakani, S. M. Davachi, Z. Bagher et al., "Fabrication of chitosan/polyvinylpyrrolidone hydrogel scaffolds containing PLGA microparticles loaded with dexamethasone for biomedical applications," *International Journal of Biological Macromolecules*, vol. 164, pp. 356–370, 2020.

[30] S. Ata, A. Rasool, A. Islam et al., "Loading of cefixime to pH sensitive chitosan based hydrogel and investigation of controlled release kinetics," *International Journal of Biological Macromolecules*, vol. 155, pp. 1236–1244, 2020.

[31] J. Li, X. Hao, C. Wang et al., "Improving the solubility, dissolution, and bioavailability of metronidazole via cocrystallization with ethyl gallate," *Pharmaceutics*, vol. 13, no. 4, p. 546, 2021.

[32] M. Okuda, Y. Lin, C. Wang, T. Kakiuchi, and S. Kikuchi, "Metronidazole for *Helicobacter pylori* eradication therapy among children and adolescents in Japan: overcoming controversies and concerns," *Helicobacter*, vol. 24, no. 3, article e12575, 2019.

[33] S. Noor, F. B. A. Salam, H. N. Hima, M. S. I. Bhuiyan, and S. S. Chowdhury, "Comparative in-vitro quality evaluation of some brands of metronidazole tablet available in Bangladesh," *International Journal of Applied Research*, vol. 3, no. 7, pp. 753–758, 2017.

[34] M. K. Katual, "Formulation, optimization and in-vitro evaluation of metronidazole 50 mg floating tablets for the treatment of helicobacter pylori induced gastric inflammatory disorder," *World Journal of Pharmaceutical Research*, vol. 6, pp. 809–835, 2017.

[35] N. Gull, S. M. Khan, S. Khalid et al., "Designing of biocompatible and biodegradable chitosan based crosslinked hydrogel for in vitro release of encapsulated povidone-iodine: a clinical translation," *International Journal of Biological Macromolecules*, vol. 164, pp. 4370–4380, 2020.

[36] M. Marques, R. Löbenberg, and M. Almukainzi, "Simulated biological fluids with possible application in dissolution testing," *Dissolution Technologies*, vol. 18, no. 3, pp. 15–28, 2011.

[37] A. Avella, J.-M. Raquez, and G. Lo Re, "Substantial effect of water on radical melt crosslinking and rheological properties of poly (ε-caprolactone)," *Polymers*, vol. 13, no. 4, p. 491, 2021.

[38] P. P. Rade, P. S. Giram, A. A. Shitole, N. Sharma, and B. Garnaik, "Physicochemical and in vitro antibacterial evaluation of metronidazole loaded Eudragit S-100 nanofibrous

mats for the intestinal drug delivery," *Advanced Fiber Materials*, vol. 4, no. 1, pp. 76–88, 2021.

[39] C. L. Narayana Reddy, B. Y. Swamy, C. V. Prasad et al., "Development and characterization of chitosan-poly (vinyl pyrrolidone) blend microspheres for controlled release of metformin hydrochloride," *International Journal of Polymeric Materials and Polymeric Biomaterials*, vol. 61, no. 6, pp. 424–436, 2012.

[40] E. Nematollahi, M. Pourmadadi, F. Yazdian, H. Fatoorehchi, H. Rashedi, and M. Navaei, "Synthesis and characterization of chitosan/polyvinylpyrrolidone coated nanoporous γ-alumina as a pH-sensitive carrier for controlled release of quercetin," *International Journal of Biological Macromolecules*, vol. 183, pp. 600–613, 2021.

[41] E. Marsano, E. Bianchi, S. Vicini et al., "Stimuli responsive gels based on interpenetrating network of chitosan and poly(vinylpyrrolidone)," *Polymer*, vol. 46, no. 5, pp. 1595–1600, 2005.

[42] M. V. Risbud, A. J. Jenkins, S. V. Bhat, and R. R. Bhonde, "pH-sensitive freeze-dried chitosan-polyvinyl pyrrolidone hydrogels as controlled release system for antibiotic delivery," *Journal of Controlled Release*, vol. 68, no. 1, pp. 23–30, 2000.

[43] F. Seidi, M. Khodadadi Yazdi, M. Jouyandeh et al., "Chitosan-based blends for biomedical applications," *International Journal of Biological Macromolecules*, vol. 183, pp. 1818–1850, 2021.

[44] J. R. Khurma, D. Rohindra, and A. V. Nand, "Swelling and thermal characteristics of genipin crosslinked chitosan and poly (vinyl pyrrolidone) hydrogels," *Polymer Bulletin*, vol. 54, no. 3, pp. 195–204, 2005.

[45] M. El Achaby, Y. Essamlali, and N. El Miri, "Graphene oxide reinforced chitosan/polyvinylpyrrolidone polymer bio-nanocomposites," *Journal of Applied Polymer Science*, vol. 131, no. 22, 2014.

[46] E. Budianto and A. R. Amalia, "Swelling behavior and mechanical properties of chitosan-poly (N-vinyl-pyrrolidone) hydrogels," *Journal of Polymer Engineering*, vol. 40, no. 7, pp. 551–560, 2020.

[47] E. S. Costa-Júnior, E. F. Barbosa-Stancioli, H. S. Mansur, W. L. Vasconcelos, and H. S. Mansur, "Preparation and characterization of chitosan/poly(vinyl alcohol) chemically crosslinked blends for biomedical applications," *Carbohydrate Polymers*, vol. 76, no. 3, pp. 472–481, 2009.

[48] T. Peng, K. Yao, C. Yuan, and M. F. A. Goosen, "Structural changes of pH-sensitive chitosan/polyether hydrogels in different pH solution," *Journal of Polymer Science Part A*, vol. 32, no. 3, pp. 591–596, 1994.

[49] A. Rahma, M. Munir, V. S. Khairurrijal, and H. Rachmawati, "Intermolecular interactions and the release pattern of electrospun curcumin-polyvinyl(pyrrolidone) fiber," *Biological & Pharmaceutical Bulletin*, vol. 39, no. 2, pp. 163–173, 2016.

[50] K. Afriani and T. S. Budikania, "Synthesis and characterization of hydrogel of chitosan-poly (N-vinyl-2-pirrolidone) (PVP)-alginate for ibuprofen release," *The Journal of Pure and Applied Chemistry Research*, vol. 9, no. 3, pp. 201–211, 2020.

[51] T. Wang, M. Turhan, and S. Gunasekaran, "Selected properties of pH-sensitive, biodegradable chitosan–poly(vinyl alcohol) hydrogel," *Polymer International*, vol. 53, no. 7, pp. 911–918, 2004.

[52] B. K. Heragh, S. Javanshir, G. R. Mahdavinia, and R. Vertesi, "Development of pH-sensitive biomaterial-based nanocomposite for highly controlled drug release," *Results in Materials*, vol. 16, p. 100324, 2022.

[53] A. Myhal, O. Golovchenko, T. L. Krutskikh, S. Gubar, and V. Georgiyants, "IR-spectroscopy research into the structure of products of interaction between metronidazole and metal salts," *Der Pharma Chemica*, vol. 8, no. 19, pp. 148–154, 2016.

[54] F. Naseem, S. U. Shah, A. Rashid, A. Farid, M. Almehmadi, and S. Alghamdi, "Metronidazole based floating bioadhesive drug delivery system for potential eradication of H. pylori: preparation and in vitro characterization," *Polymers*, vol. 14, no. 3, p. 519, 2022.

[55] E. A. Mogilevskaya, T. A. Akopova, A. N. Zelenetskii, and A. N. Ozerin, "The crystal structure of chitin and chitosan," *Polymer Science Series A*, vol. 48, no. 2, pp. 116–123, 2006.

[56] K. Ogawa, T. Yui, and M. Miya, "Dependence on the preparation procedure of the polymorphism and crystallinity of chitosan membranes," *Bioscience, Biotechnology, and Biochemistry*, vol. 56, no. 6, pp. 858–862, 1992.

[57] K. Lewandowska, "Miscibility and interactions in chitosan acetate/poly(N-vinylpyrrolidone) blends," *Thermochimica Acta*, vol. 517, no. 1–2, pp. 90–97, 2011.

[58] M. M. Beppu, R. S. Vieira, C. G. Aimoli, and C. C. Santana, "Crosslinking of chitosan membranes using glutaraldehyde: effect on ion permeability and water absorption," *Journal of Membrane Science*, vol. 301, no. 1–2, pp. 126–130, 2007.

[59] D. Archana, B. P. Singh, J. Dutta, and P. Dutta, "Chitosan-PVP-nano silver oxide wound dressing: in vitro and in vivo evaluation," *International Journal of Biological Macromolecules*, vol. 73, pp. 49–57, 2015.

[60] H. A. K. Sabbagh, S. H. Hussein-Al-Ali, M. Z. Hussein, Z. H. M. Abudayeh, R. Ayoub, and S. M. Abudoleh, "A statistical study on the development of metronidazole-chitosan-alginate nanocomposite formulation using the full factorial design," *Polymers*, vol. 12, no. 4, p. 772, 2020.

[61] H. A. K. Sabbagh, Z. Abudayeh, S. M. Abudoleh, J. A. Alkrad, M. Z. Hussein, and S. H. Hussein-Al-Ali, "Application of multiple regression analysis in optimization of metronidazole-chitosan nanoparticles," *Journal of Polymer Research*, vol. 26, no. 8, 2019.

[62] R. Poonguzhali, S. K. Basha, and V. S. Kumari, "Synthesis and characterization of chitosan-PVP-nanocellulose composites for _in-vitro_ wound dressing application," *International Journal of Biological Macromolecules*, vol. 105, no. 1, pp. 111–120, 2017.

[63] A. Nesic, J. Ružić, M. Gordić, S. Ostojić, D. Micic, and A. Onjia, "Pectin-polyvinylpyrrolidone films: a sustainable approach to the development of biobased packaging materials," *Composites Part B: Engineering*, vol. 110, pp. 56–61, 2017.

[64] R. K. Mondal, K. A. Dubey, J. Kumar et al., "Carbon nanotube functionalization and radiation induced enhancements in the sensitivity of standalone chemiresistors for sensing volatile organic compounds," *ACS Applied Nano Materials*, vol. 1, no. 10, pp. 5470–5482, 2018.

[65] M. D. Gower and R. A. Shanks, "The effect of varied monomer composition on adhesive performance and peeling master curves for acrylic pressure-sensitive adhesives," *Journal of Applied Polymer Science*, vol. 93, no. 6, pp. 2909–2917, 2004.

[66] R. S. H. Wong, M. W. Ashton, and K. Dodou, "Effect of cross-linking agent concentration on the properties of unmedicated hydrogels," *Pharmaceutics*, vol. 7, no. 3, pp. 305–319, 2015.

[67] B. N. Oshani, S. M. Davachi, I. Hejazi, J. Seyfi, H. A. Khonakdar, and A. Abbaspourrad, "Enhanced compatibility of starch with poly(lactic acid) and poly(ε-caprolactone) by incorporation of POSS nanoparticles: study on thermal properties," *International Journal of Biological Macromolecules*, vol. 141, pp. 578–584, 2019.

[68] I. A. Duceac, L. Verestiuc, C. D. Dimitriu, V. Maier, and S. Coseri, "Design and preparation of new multifunctional hydrogels based on chitosan/acrylic polymers for drug delivery and wound dressing applications," *Polymers*, vol. 12, no. 7, p. 1473, 2020.

[69] I. Sebti, A. Martial-Gros, A. Carnet-Pantiez, S. Grelier, and V. Coma, "Chitosan polymer as bioactive coating and film against *Aspergillus niger* contamination," *Journal of Food Science*, vol. 70, no. 2, pp. M100–M104, 2005.

[70] N. P. Arslan, Ö. Yilmaz, and E. Demiray-Gürbüz, "Importance of antimicrobial susceptibility testing for the management of eradication in *Helicobacter pylori* infection," *World Journal of Gastroenterology*, vol. 23, no. 16, pp. 2854–2869, 2017.

[71] X. Wu, Z. Tang, X. Liao, Z. Wang, and H. Liu, "Fabrication of alginate microspheres with porous core and compact shell, and application as a quick traumatic hemostat," *Carbohydrate Polymers*, vol. 247, p. 116669, 2020.